scientific reports

Check for updates

OPEN

Improved gated recurrent unit-based osteosarcoma prediction on histology images: a meta-heuristic-oriented optimization concept

S. Prabakaran[1]✉ & S. Mary Praveena[2]

The major prevalent primary bone cancer is osteosarcoma. Preoperative chemotherapy is accompanied by resection as part of the normal course of treatment. The diagnosis and treatment of patients are based on the chemotherapy reaction. Contrarily, chemotherapy without operation results in persistent cancer and an osteosarcoma regrowth. Thus, osteosarcoma patients should receive comprehensive therapy, which includes tumor-free surgery and global chemotherapy, to improve their survival. Hence, early diagnosis and individualized care of osteosarcoma are essential since they may lead to more effective therapies and higher survival rates. Here, the main goal of the recommended research is to use a unique deep learning approach to predict the osteosarcoma on histology images. Initially, the data is collected from the navigation confluence mobile osteosarcoma data of UT Southwestern/ UT Dallas dataset. Next, the pre-processing of the collected images is accomplished by the Weiner filter technique. Further, the segmentation for the pre-processed images is done by the 2D Otsu's method. From the segmented images, the features are extracted by the linear discriminant analysis (LDA) approach. These extracted features undergo the final prediction phase that is accomplished by the novel improved recurrent gated recurrent unit (IGRU), in which the parameter tuning of GRU is accomplished by the osprey optimization algorithm (OOA) with the consideration of error minimization as the major objective function. On contrast with various conventional methods, the simulation findings demonstrate the effectiveness of the developed model in terms of numerous analysis.

Keywords Osteosarcoma prediction, Histology images, Improved gated recurrent unit, Osprey optimization algorithm

Abbreviations

LDA	Linear discriminant analysis
CAD	Computer-assisted detection
MAPE	Mean absolute percentage error
IGRU	Improved gated recurrent unit
CT	Computed tomography
OOA	Osprey optimization algorithm
MRI	Magnetic resonance imaging
CE FS T1-w	Contrast-enhanced fat-suppressed T1-weighted
PS	Prognostic score
LASSO	Least absolute shrinkage and selection operator
RMSE	Root mean square error
lncRNAs	Long non-coding RNAs
LR	Logistic regression
EHO	Elephant herding optimization
CRLncs	Cuproptosis-related LncRNAs
WSIs	Whole slide images
SMAPE	Symmetric mean absolute percentage error

[1]Department of ECE, CMS College of Engineering and Technology, Coimbatore, Tamilnadu 641032, India. [2]Department of ECE, Sri Ramakrishna Institute of Technology, Coimbatore, Tamilnadu 641022, India. ✉email: sprabakaran87@gmail.com

TME	Tumor micro environment
GBA	Guilt by association
T/B	Tumor to background ratio
GO	Gene ontology
SFO	Sun flower optimization
WR	Washout rate
DEGs	Differentially expressed genes
AR	Alteration rate
DCN	Differential co-expression network
GOA	Grasshopper optimization algorithm
TARGET	Therapeutically applicable research to generate effective treatments
SCC	Spearman correlation coefficient
PSD	Power spectral density
AUC	Area under the curve
MSE	Mean square error
SNR	Signal-to-noise ratio
MVO	Multi verse optimization
ROC	Receiver operating characteristic

An osteosarcoma, also known as osteogenic sarcoma, describes a kind of bone cancer that commonly develops in the long bones[1]. It may develop in any bone cells. Under extremely uncommon circumstances, it may even harm the tissues that surround the bones. Although it can affect persons of various ages as well, it primarily impacts adolescents and young adults. The typical age of detection for osteosarcoma is 15 years old[2]. It represents the most common type of malignant tumor to develop in young people. Guys as well as girls are approximately similarly prone to infection up until late adolescence, or ages 15 to 19, however after that point, guys are more commonly afflicted and at risk of having their bone cells destroyed. Although osteosarcoma has no known origin and normally does not run in relationships, it develops because of a flaw in the gene that may create illness, just like various types of cancer[3]. Additionally, it has been connected to situations when familial retinoblastoma, a form of pediatric eye cancer, runs in the bloodline. Adolescent osteosarcoma describes a serious danger for children with family retinoblastoma[4]. The disease's typical signs involve discomfort in the damaged bone, which starts off mildly before getting worse with time[5]. Bone fracture represents one among the various signs because the damaged bone fractures as a result of getting infected and diminishing strength.

The identification of osteosarcomas describes a challenging and time-consuming procedure that requires extensive training[6]. The health industry has adopted computerized detection procedures as a result of developing novel approaches and speedy processing technology. These frameworks typically consist of a feature extractor that uses the features as input, accompanied by a classifier[7]. Before the feature extractor, certain frameworks could additionally include a pre-processing phase[8]. This pre-processing can include noise-reduction filters, contrast enhancement, and various techniques[9]. Researchers have proven the creation of CAD frameworks as a method for segmenting and identifying osteosarcoma utilizing a variety of images, involving CT and MRI tests. However, CT as well as MRI scans have drawbacks[10]. The osteosarcoma can be illustrated as shown in (Fig. 1) below.

The issue of inadequate medical diagnostic accuracy for osteosarcoma in underdeveloped nations has somewhat improved with the development of intelligent technology[11]. This methodology automatically segments images of osteosarcoma in determining the existence and condition of osteosarcoma[12]. It does this by using deep learning, template matching, edge detection, and various techniques to identify key targets in MRI images. On the margin of the osteosarcoma, nevertheless, there will also be certain local tissue development, which results in ambiguous and confusing tumor boundaries. As a result of the difficult anatomical format and irregular form of osteosarcoma images, as well as the varied imaging techniques and the availability of noise in the image, segmentation results are frequently unacceptable[13]. Investigators carry out a significant count in order to enhance the precision[14]. Nevertheless, the segmentation parameter number and complexity are enhanced, and the inference performance is extremely sluggish[15]. Yet, a disadvantage of these methods is their high processing and information needs.

The main contributions of this research are as follows:

- A novel deep learning framework, IGRU is introduced, integrated with the osprey optimization algorithm (OOA) for efficient parameter tuning and error minimization.
- An advanced preprocessing pipeline using Wiener filter and 2D Otsu method is implemented to enhance the quality of histopathological images for prediction.
- LDA is utilized for feature extraction, addressing challenges associated with noisy and high-dimensional medical image data.
- The proposed methodology is validated on a benchmark dataset, demonstrating significant improvements in prediction accuracy (92.3%) compared to existing methods.
- A comprehensive evaluation using multiple metrics and comparative analysis against state-of-the-art models confirms the superiority of the IGRU-OOA framework.
- The introduction of the OOA metaheuristic optimization framework adds significant novelty, balancing exploration and exploitation for parameter optimization.
- The study addresses clinical relevance by enabling accurate early prediction of osteosarcoma, supporting personalized treatment plans and improving patient outcomes.

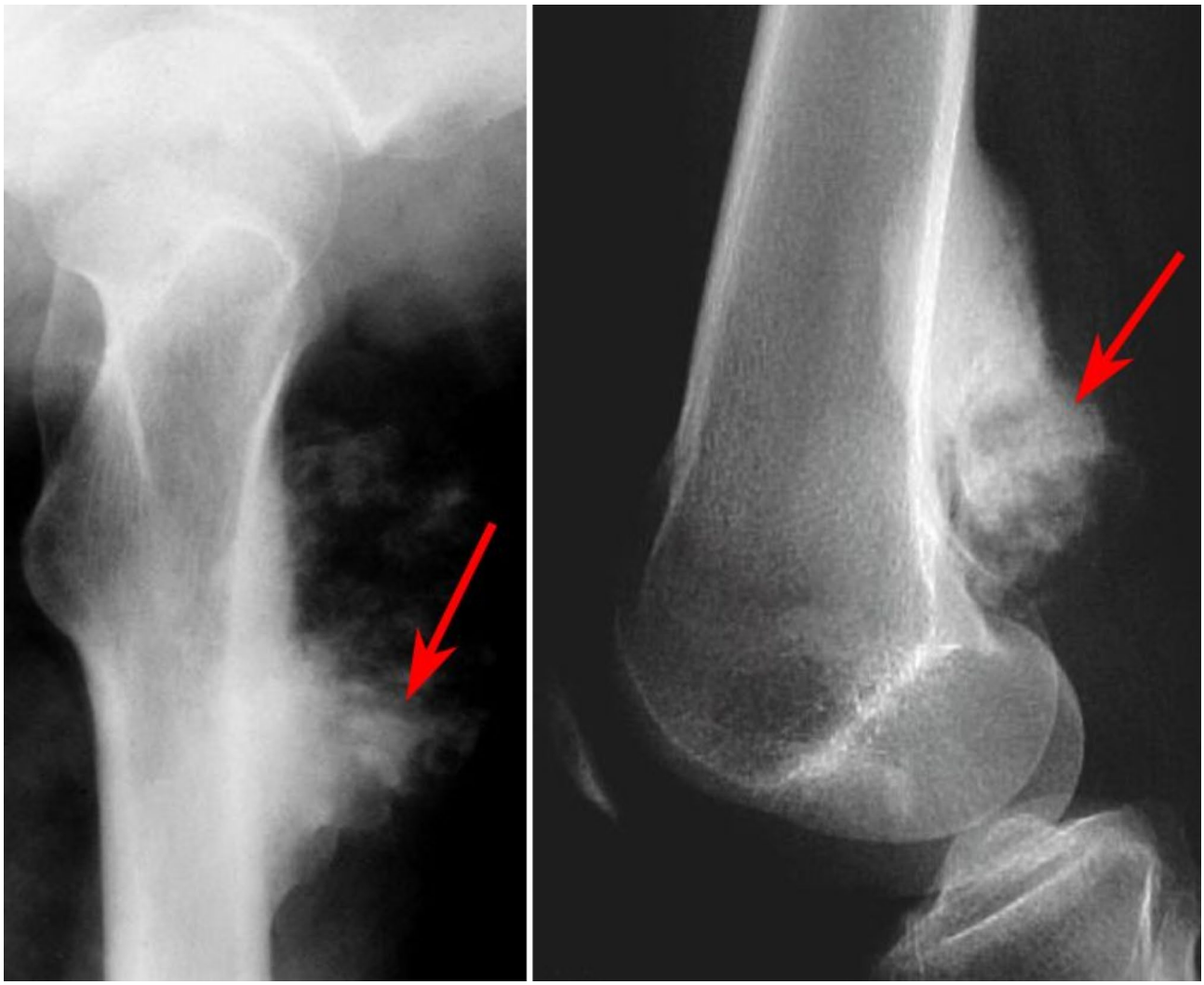

Fig. 1. Diagrammatic illustration of osteosarcoma.

The paper organization is. Section I shows the introduction of the osteosarcoma prediction model. Section II is literature survey. Section III is data collection and pre-processing for the developed osteosarcoma prediction model. Section IV is segmentation and feature extraction for the developed osteosarcoma prediction model. Section V is prediction stage and optimization algorithm for the developed osteosarcoma prediction model. Section VI is results. Section VII is conclusion.

Literature survey

Related works

Fauzi et al.[16] explored the reliability of laboratory, clinical, and MRI data in osteosarcoma patients, using a cross-sectional observational model to compare tumor necrosis proportions before and after neoadjuvant treatment. Chen et al.[17] developed an MR-based radiomics nomogram to predict early relapse in osteosarcoma after surgery and chemotherapy, leveraging LASSO regression for feature selection and multivariate logistic regression for prognosis. Zhang et al.[18] proposed a prognostic methodology identifying RNA signatures for recurrence prediction, supported by Kaplan-Meier survival analysis and pathway enrichment. Wang et al.[19] identified lncRNAs linked to cuproptosis using RNA sequencing and functional studies, categorizing patients into risk groups to evaluate tumor microenvironment and therapy responses. In 2023, Ho et al.[20] proposed a deep learning-based method utilizing hematoxylin and eosin-stained whole slide images (WSIs) to evaluate necrosis ratios for predicting osteosarcoma outcomes. The study analyzed 3134 WSIs from 103 patients and trained a Deep Multi-Magnification framework to segment tissue subtypes, including viable and necrotic tumors. The model's calculated necrosis ratios strongly correlated with specialist evaluations and successfully stratified patients to predict survival and progression-free longevity. Xinrang Chen[21] introduced a network-oriented gene function inference methodology based on the guilt-by-association (GBA) concept to estimate optimal gene functions for osteosarcoma. Differentially expressed genes (DEGs) were identified using LIMMA software, and a differential co-expression network (DCN) was constructed, followed by sub-DCN extraction

using the Spearman Correlation Coefficient. Gene Ontology (GO) labels were then applied to predict gene functions, with the model's performance assessed using the area under the curve (AUC).

Wu et al.[22] developed a radiomics nomogram for predicting survival in high-grade osteosarcoma (HOS) using CT images. Radiomic features were extracted and used to create a radiomics signature via LASSO regression, which was combined with medical parameters to form a predictive nomogram. Validated on a cohort of 48 patients, the radiomics nomogram outperformed traditional clinical methodologies in classification and calibration capacity. Caixia et al.[23] explored the use of dual imaging with 99mTc-MIBI scintigraphy to predict and assess responses to neoadjuvant chemotherapy in osteosarcoma patients. This study involved 30 patients who underwent imaging before and after treatment, demonstrating the potential of this approach for treatment evaluation.

Yu et al.[24] utilized univariate and multivariate Cox proportional hazards regression analyses to identify long non-coding RNAs (lncRNAs) associated with osteosarcoma survival. Kaplan-Meier survival curves and time-dependent ROC analysis were employed to validate predictive lncRNAs, with the AUC used to confirm their prognostic significance. Similar such metaheuristic approaches have been investigated in literatures[25–27].

Zhong et al.[28] focused on diagnosing and evaluating osteosarcoma cell functions through PCR-based analysis. Their work validated cell distribution using microscopy and assessed cell viability through assays, providing foundational insights into osteosarcoma cellular behavior. Data collection and pre-processing for the developed osteosarcoma prediction model.

While the existing methods in the literature demonstrate advancements in osteosarcoma prediction, they have notable limitations. Approaches like radiomics-based nomograms and deep learning frameworks often rely on extensive feature extraction processes that may not adequately handle the complexity and noise in histopathological data. For example, models like the radiomics nomogram proposed by Wu et al.[22] depend heavily on manual or semi-automated feature engineering, which can introduce variability and limit reproducibility. Similarly, segmentation techniques, such as those in Ho et al.[20], are effective but computationally intensive, potentially hindering real-time clinical deployment. Methods that integrate molecular biomarkers, such as the work of Yu et al.[24] and Wang et al.[19], often lack robustness in handling diverse datasets or addressing the intricacies of high-dimensional data. Seyedali Mirjalili et al.[29] presents the Multi-Verse Optimizer (MVO), a technique inspired by cosmological concepts like white holes, black holes, and wormholes. The algorithm's merits include robust exploration and exploitation capabilities, demonstrated through competitive benchmarking on 19 test problems and real-world engineering scenarios, outperforming algorithms like PSO and GA. However, its computational complexity and dependency on parameter settings are noted limitations. The work highlights MVO's potential for solving diverse optimization challenges effectively. Kaplan-Meier survival curves and time-dependent ROC analysis were employed to validate predictive lncRNAs, with the AUC used to confirm their prognostic significance. Similar such metaheuristic approaches have been investigated in literatures[30–32] Mohammed et al.[33] introduces an Automated Osteosarcoma Detection and Classification using metaheuristics with Advanced Deep Learning (AODC-MADL) algorithm. The proposed AODC-MADL model makes use of recent DL models with hyperparameter optimization algorithms to detect and classify osteosarcoma.

The proposed work addresses these gaps by introducing an improved gated recurrent Unit (IGRU) model optimized through the osprey optimization algorithm (OOA). This framework combines advanced preprocessing techniques, such as Wiener filtering and 2D Otsu-based segmentation, with robust feature extraction using linear discriminant analysis (LDA). By leveraging the IGRU's capability to learn temporal dependencies and OOA's parameter optimization, the proposed model minimizes prediction errors while handling noisy, high-dimensional data effectively. Additionally, the incorporation of a benchmark dataset ensures generalizability, and the streamlined pipeline reduces computational overhead, enabling real-time applicability. These innovations position the proposed work as a comprehensive solution to the limitations of existing methods, paving the way for more accurate and reliable osteosarcoma prediction.

Proposed model

The proposed osteosarcoma prediction model is composed of various phases including data collection, pre-processing, segmentation, feature extraction, and prediction. In the first phase referred to as data collection, the images associated with the osteosarcoma are gathered from the Navigation Confluence Mobile osteosarcoma data of UT Southwestern/UT Dallas dataset. Next to the data collection, the pre-processing of the gathered images is accomplished by the Weiner filter technique. For these pre-processed images, the segmentation is done using the 2D Otsu's method. The features are extracted from these segmented images with the help of LDA approach. In the final phase, the prediction is accomplished for these extracted features using novel IGRU, where the parameter tweaking in GRU is performed by the OOA with the intention of error minimization as the major objective function. The IGRU returns the final predicted output. The complete diagram of the recommended osteosarcoma prediction model is illustrated in (Fig. 2) below.

Data collection

For empirical validation, a benchmark navigation confluence mobile osteosarcoma dataset from UT Southwestern/UT Dallas is used. Osteosarcoma describes the major kind of bone cancer within adolescents. Osteosarcoma histopathological images having H&E labels make up the assortment. Individuals are chosen by physicians after the procedure. The database contains 1144 images having a 10X resolution and a 1024 by 1024 size. Images are distributed beneath: 263 (23%) non-viable tumor tiles, 536 (47%) non-tumor images, and 345 (30%) viable tumor tiles.

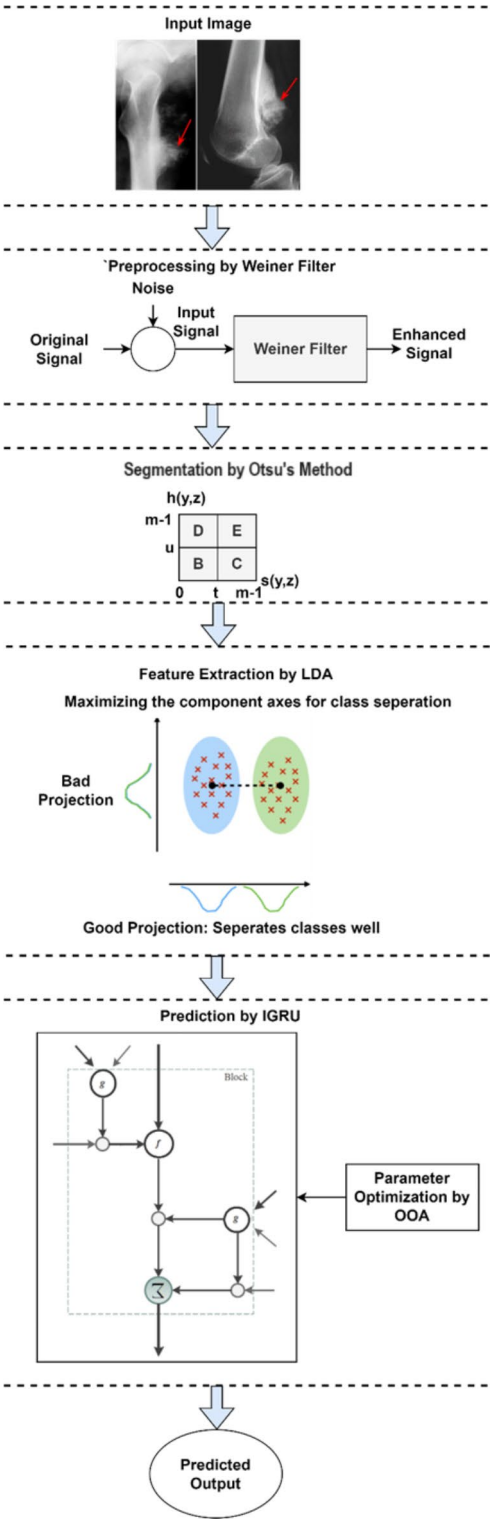

Fig. 2. Complete diagram of the recommended osteosarcoma prediction model.

Pre-processing

The pre-processing for the developed osteosarcoma prediction model is accomplished by the Weiner filter technique. The Wiener filter's goal is to eliminate noise that has caused a signal to become deformed. An experimental technique backs it up. A filter's typical response to noise is constructed. When it applies to filtering, the Wiener filter has a unique approach. Assuming one has knowledge associated with the spectral properties of the original signal plus the noise, one looks for the linear time invariant filter whose output will appear as identical to the real signal as possible. the following Wiener filter features:

- It is presumed that the noise plus the signal are both additive, stationary, linear random processes with familiar spectrum features.
- The filter should be actually realizable, or causal, according to the need (this condition may be waived for a non-causal approach).
- Minimum mean-square error is the efficiency criterion.

The Wiener filter is as below:

$$H(v,w) = \frac{I*(v,w)\,Q_t(v,w)}{|I(v,w)|^2 Q_t(v,w) + Q_o(v,w)} \tag{1}$$

By dividing via by Q_t, its behavior becomes more understandable:

$$H(v,w) = \frac{I*(v,w)}{|I(v,w)|^2 + Q_o(v,w)/Q_t(v,w)} \tag{2}$$

Here, PSD of un-degraded image is shown by $Q_t(v,w)$, PSD of noise is shown by $Q_o(v,w)$, complex conjugate associated with the degradation function is shown by $I*(v,w)$, and degradation function is shown by $I(v,w)$ respectively. The symbol $Q_o/Q_t$is equivalent to the SNR in reverse. These attained pre-processed images are subjected to the 2D Otsu's method in order to perform the process of segmentation.

Segmentation and feature extraction for the developed osteosarcoma prediction model

Segmentation

The segmentation for the pre-processed images of the introduced osteosarcoma model is accomplished by the 2D Otsu's method. Provided an image with the dimensions $g(y,z)$and M grey levels, and O total pixels in the image. Assume M grey levels describe the neighborhood average image, $h(y,z)$, as seen in the image.

We may get a pair (j,k) for every pixel in the image, in which j represents the original grey level that showed in $g(y,z)$, and k represents the neighbourhood average grey level that occurred in $h(y,z)$. Assume d_{jk} stand for the frequency of the pair (j,k), then its joint probability may be written as $q_{jk} = \frac{d_{jk}}{O}$, in which j and k are denoted by $0,1,\cdots,M-1$, and $\sum_{j=0}^{M-1}\sum_{k=0}^{M-1} q_{jk} = 1$.

Provided a threshold vector (t,u) of any size. The 2D histogram is divided into four areas by this threshold vector. The item is represented by areas B while the backdrop is represented by areas E. Edges as well as noise are described by areas C and D. Consider there are two classes, $D_0$and D_1, which stand in for the object as well as the backdrop, correspondingly. Then, assume that there are two classes D_j, ω_j and $\mu_j$which stand in for the probability as well as mean value vectors, correspondingly. The likelihoods of $D_0$and D_1may be expressed as

$$\omega_0 = \sum_{j=0}^{t}\sum_{k=0}^{u} q_{jk} \tag{3}$$

$$\omega_1 = \sum_{j=t+1}^{M-1}\sum_{k=u+1}^{M-1} q_{jk} \tag{4}$$

It is possible to describe the mean value vectors of $D_0$and D_1as

$$\mu_0 = \left(\mu_{0j}, \mu_{0k}\right)^T = \left(\sum_{j=0}^{t}\sum_{k=0}^{u}\frac{jq_{jk}}{\omega_0}, \sum_{j=0}^{t}\sum_{k=0}^{u}\frac{kq_{jk}}{\omega_0}\right)^T \tag{5}$$

$$\mu_1 = \left(\mu_{1j}, \mu_{1k}\right)^T = \left(\sum_{j=t+1}^{M-1}\sum_{k=u+1}^{M-1}\frac{jq_{jk}}{\omega_1}, \sum_{j=t+1}^{M-1}\sum_{k=u+1}^{M-1}\frac{kq_{jk}}{\omega_1}\right)^T \tag{6}$$

The 2D histogram's overall mean vector is

$$\mu_T = \left(\mu_{Tj}, \mu_{Tk}\right)^T = \left(\sum_{j=0}^{M-1}\sum_{k=0}^{M-1} jq_{jk}, \sum_{j=0}^{M-1}\sum_{k=0}^{M-1} kq_{jk}\right)^T \tag{7}$$

The likelihood that is distant from the diagonal is often quite small. It may quickly confirm the relationships $\omega_0 + \omega_1 \approx 1$ and $\mu_T \approx \omega_0\mu_0 + \omega_1\mu_1$. The definition of the between-class discrete matrix is

$$T_c = \sum_{l=0}^{1}\left[(\mu_l - \mu_T)(\mu_l - \mu_T)^T\right] \tag{8}$$

The discrete matrix's trace may be represented as

$$UsT_c(t,u) = \sum_{l=0}^{1}\left(\left[\left(\mu_{lj} - \mu_{Tj}\right)^2 + \left(\mu_{lk} - \mu_{Tk}\right)^2\right]\right) \tag{9}$$

Therefore, the ideal threshold is described as

$$(t^*, u^*) = \arg \underbrace{max}_{0 \le t,\ u \le M-1} UsT_c(t, u) \tag{10}$$

It should be noted that pixels that meet the requirements $g(y,z) \le t^*$and $h(y,z) > u^*$and $g(y,z) > t^*$and $h(y,z) \le u^*$are disregarded and are assigned to either 0 or 1. The final segmented images are given as input to the LDA methodology in order to extract the features.

Feature extraction

The feature extraction for the segmented images of the developed osteosarcoma prediction model is accomplished by the LDA approach. In order to maximize between-class scatter while concurrently minimizing within-class scatter, LDA seeks to identify a collection of projection vectors.

Assume $Y \in S^{q \times o}$, in which q shows the count of features and o shows the count of samples, be a sample matrix with the columns $y_j \in S^q,\ j = 1, \cdots, o$. The definitions of the within-class scatter matrix $T_x$and the between-class scatter matrix $T_c$are

$$T_c = \frac{1}{o} \sum {}_{l=1}^{d} o_l \left(n^{(l)} - n\right) \left(n^{(l)} - n\right)^T \tag{11}$$

$$T_x = \frac{1}{o} \sum {}_{l=1}^{d} \sum {}_{k=1}^{o_l} \left(y_k^{(l)} - n^{(l)}\right) \left(y_k^{(l)} - n^{(l)}\right)^T \tag{12}$$

Here, d denotes the count of classes, $o_l$the count of samples in class l, $y_k^{(l)}$ the k^{th}sample in class l, and $n^{(l)}$ and n, correspondingly, denote the mean vector of class l and the overall mean vector. The projection matrix X that maximises the Fisher criteria is next discovered via LDA.

$$K_{LDA}(X) = trace\left(\left(X^T T_x X\right)^{-1} \left(X^T T_c X\right)\right) \tag{13}$$

Susceptible to restrictions such as the orthogonality requirement on X, or $X^T X = J$. X may be discovered as the eigenvectors of $T_x^{-1} T_c$that relate to the biggest eigenvalues by addressing a generalized eigenvalue issue. The extracted features from the LDA approach are given to the IGRU that in turn performs the final prediction phase of the developed osteosarcoma prediction model.

Prediction stage and optimization algorithm for the developed osteosarcoma prediction model

Proposed IGRU

The proposed novel IGRU is used for performing the final prediction phase, in which the parameter optimization in GRU is done by the OOA with the consideration of error minimization as the major objective function. To enable recurrent blocks to adaptively record the interdependence of various time scales, the GRU was suggested. $tanh$ or sigmoid functions are frequently used as activation functions ("g", "h"). In the k^{th}GRU, the prospective update $\tilde{i}{}_u^k$must be determined initially when provided an input vector $y_u$at time u:

$$\tilde{i}{}_u^k = tanh(X y_u + V(s_u \otimes i_{u-1}))^k \tag{14}$$

Here, $\otimes$ shows an element-wise multiplication operation and a group of reset gates s_u regulates how much each unit updates from all of the earlier activations of the identical layer's units i_{u-1}. A reset gate $s_u^k$is calculated using:

$$s_u^k = \sigma\left(X_s y_u + V_s i_{u-1}\right)^k \tag{15}$$

A sigmoid function describes the activation function σ. The GRU is next activated based on its most recent candidate update and its prior activation:

$$i_u^k = \left(1 - a_u^k\right) i_{u-1}^k + a_u^k \tilde{i}{}_u^k \tag{16}$$

Here, the update gate a_u^k, which is determined as follows, determines how much the unit updates upon its activation:

$$a_u^k = \sigma\left(X_a y_u + V_a i_{u-1}\right)^k \tag{17}$$

The number of gates is decreased in GRU. GRU gates can only be activated based on their present input and past output. GRU methods typically converge more quickly and produce better results as a result of the fewer parameters used. Still, memory cell does not exist in GRU. Hence, to overcome the limitation, the parameter tweaking is accomplished by OOA, thus referred as novel IGRU. This novel IGRU predicts the final outcome of the developed osteosarcoma model.

OOA

The OOA is used for tuning the parameters of the GRU in order to derive error minimization as the major objective function. OOA mimics osprey behavior in the wild. Ospreys' method of marine fish hunting serves as the main model for OOA. With this method of hunting, the osprey chases the prey after locating it, next transports it to an appropriate location for consumption. The computational representation of the developed OOA technique, which entails two stages of exploration and exploitation, is dependent on a simulation of the natural behavior of ospreys throughout the hunting procedure. Here, the parameters of OOA describe the parameters of the GRU model that is employed to perform the developed osteosarcoma prediction model.

The suggested OOA defines a population-oriented strategy that, using a repetition-oriented method, may find a workable solution on the basis of the search power of its population members in the problem-solving space. Every osprey chooses values for the issue variables depending on its location in the search space as a member of the OOA population. As a result, every osprey represents a potential solution to the issue, represented numerically as a vector. The OOA population, which is made up of all ospreys, may be modelled utilizing a matrix in accordance with (18). Employing (19), the location of ospreys in the search space is initialized at random at the start of OOA development.

$$Y = \begin{bmatrix} Y_1 \\ \vdots \\ Y_j \\ \vdots \\ Y_O \end{bmatrix}_{O\times n} = \begin{bmatrix} y_{1,1} & \cdots & y_{1,k} & \cdots & y_{1,n} \\ \vdots & \ddots & \vdots & \iddots & \vdots \\ y_{j,1} & \cdots & y_{j,k} & \cdots & y_{j,n} \\ \vdots & \iddots & \vdots & \ddots & \vdots \\ y_{O,1} & \cdots & y_{O,k} & \cdots & y_{O,n} \end{bmatrix}_{O\times n} \tag{18}$$

$$y_{j,k} = LB_k + s_{j,k} \cdot \left(UB_k - LB_k\right),\ j = 1,2,\cdots,O,\ k = 1,2,\cdots,n \tag{19}$$

Here, Y_j shows the j^{th} osprey referred to as a candidate solution, $y_{j,k}$ shows its k^{th} dimension referred as problem variable, O shows the count of ospreys, n shows the count of problem variables, $s_{j,k}$describes random numbers in the range [0, 1], $LB_k$and UB_krepresents the lower bound as well as upper bound of the k^{th} problem variable, correspondingly, and Y shows the population matrix of the positions of the ospreys.

The objective function may be assessed since every osprey represents a potential solution to the issue, matching every osprey. A vector may be used to describe the evaluated values for the problem's objective function, as per (20).

$$G = \begin{bmatrix} G_1 \\ \vdots \\ G_j \\ \vdots \\ G_O \end{bmatrix}_{O\times 1} = \begin{bmatrix} G(Y_1) \\ \vdots \\ G(Y_j) \\ \vdots \\ G(Y_O) \end{bmatrix}_{O\times 1} \tag{20}$$

Here, $G_j$shows the calculated objective function value for the j^{th}element and G shows the vector containing the objective function values. The primary criterion for assessing the calibre of potential solutions is the estimated values for the objective function. The optimal candidate solution (i.e., the optimal member) relates to the optimal value found for the objective function, while the worst candidate solution (i.e., the worst member) relates to the worst value attained for the objective function. The optimal candidate solution should be modified in every iteration since the position related to the ospreys in the search space is modified on every iteration.

Owing to their keen eyesight, ospreys represent formidable hunters who can locate fish underwater. They locate the fish, attack it, and chase the fish by diving beneath the surface. On the basis of a simulation of these ospreys' typical behavior, the initial stage of the population upgrade in OOA is modelled. The position related to the osprey in the search space varies significantly as a result of modelling the osprey attack on fish, increasing the exploration capacity of OOA in locating the ideal location and eluding the local optima.

The placements of remaining ospreys in the search space that include a higher objective function value are regarded as undersea fishes for every osprey in OOA model. Utilizing (21), the group of fish for every osprey is defined.

$$GQ_j = \left\{Y_l | l \in \{1,2,\cdots,O\}_l^G < G_j\right\} \cup \{Y_{Best}\} \tag{21}$$

Here, Y_{Best} shows the optimal candidate solution (the optimal osprey) and GQ_jshows the collection of fish locations for the j^{th} osprey. One among these fish is randomly located by the osprey, which then strikes it. A novel location for the relevant osprey is determined utilizing (22) and (23) on the basis of the computerized modelling of the migration of the osprey approaching the fish. If the value associated with the objective function is enhanced, this novel location will take the position of the osprey's former one.

$$y_{j,k}^{Q1} = y_{j,k} + s_{j,k} \cdot \left(TG_{j,k} - J_{j,k} \cdot y_{j,k}\right) \tag{22}$$

$$y_{j,k}^{Q1} = \begin{cases} y_{j,k}^{Q1}, & LB_k \le y_{j,k}^{Q1} \le UB_k \\ LB_k, & y_{j,k}^{Q1} < LB_k \\ UB_k, & y_{j,k}^{Q1} > UB_k \end{cases} \tag{23}$$

$$Y_j = \begin{cases} Y_j^{Q1}, & G_j^{Q1} < G_j \\ Y_j, & else \end{cases} \tag{24}$$

Here, Y_j^{Q1} shows the novel location of the j^{th} osprey on the basis of the initial stage of OOA, $y_{j,k}^{Q1}$ shows its k^{th} dimension, G_j^{Q1} shows its objective function value, TG_j show the chosen fish for j^{th} osprey, $TG_{j,k}$ defines the its k^{th} dimension, $s_{j,k}$ describes random numbers in the interval [0, 1], and $J_{j,k}$j represents random numbers from the set {1, 2}.

The osprey brings the fish it has just caught to an appropriate (and safe) location so that it may be eaten. On the basis of a simulation of this osprey's real behavior, the next stage of upgrading the population in OOA is modelled. The osprey's location in the search space is slightly altered as an outcome of the modelling of dragging the fish to the proper location, which increases the OOA's exploitation power in the local search and causes convergence in the path of better solutions close to the newly found solutions.

In the OOA methodology, a novel random location is initially determined for every member of the population as an "appropriate location for consuming fish" utilizing (25) and (26) in order to imitate this natural behavior of ospreys. Next, in accordance with (27), it substitutes the former location of the related osprey if the value of the goal function is enhanced in this novel location.

$$y_{j,k}^{Q2} = y_{j,k} + \frac{LB_k + s \cdot (UB_k - LB_k)}{u},\ j = 1,2,\cdots,O,\ k = 1,2,\cdots,n,\ u = 1,2,\cdots,U \tag{25}$$

$$y_{j,k}^{Q2} = \begin{cases} y_{j,k}^{Q2}, & LB_k \le y_{j,k}^{Q2} \le UB_k \\ LB_k, & y_{j,k}^{Q2} < LB_k \\ UB_k, & y_{j,k}^{Q2} > UB_k \end{cases} \tag{26}$$

$$Y_j = \begin{cases} Y_j^{Q2}, & G_j^{Q2} < G_j \\ Y_j, & else \end{cases} \tag{27}$$

Here, G_j^{Q2} shows the objective function value, Y_j^{Q2} shows the novel location of the j^{th} osprey on the basis of the second stage of OOA, $y_{j,k}^{Q2}$ shows its k^{th} dimension, $s_{j,k}$ represents random integers in the range [0, 1], u shows the algorithm's iteration timer, and U shows the total count of iterations.

The suggested OOA uses an iterative methodology. By upgrading the entire ospreys' locations in accordance with the initial and next stages, the initial iteration of OOA is finished. The optimal candidate solution is next modified on the basis of a comparison of the values of the goal function. The method next moves on to the following iteration having the revised osprey placements, and so on till the final iteration on the basis of steps (4) to (8). The optimal candidate solution saved during the iterations is finally presented by OOA as a solution to the issue when the method has been fully implemented. Algorithm 1 presents the OOA execution stages as pseudocode.

Results

Experimental setup

The developed IGRU-OOA-based osteosarcoma prediction model was implemented in Python and the results were evaluated. The population size as well as the iteration count was located as 10 and 100. The developed osteosarcoma prediction model was contrasted with distinct traditional heuristic-associated optimization methods such as multi verse optimization (MVO), elephant herd optimization (EHO), sunflower optimization (SFO), and grasshopper optimization algorithm (GOA) with consideration of distinct analyzes including MAPE, RMSE, SMAPE, MSE, and L1 Norm to describe the betterment of the developed osteosarcoma prediction model. Before evaluation, the model undergoes training and testing stages for the learning process which are discussed below.

Training phase

The training phase is where the model learns to identify relationships between input features and output predictions by iteratively adjusting its parameters. In our methodology:

- The dataset was split into 80% for training and 20% for testing to ensure a sufficient amount of data for learning while retaining enough samples for unbiased evaluation.
- The parameters of the IGRU were optimized using the Osprey Optimization Algorithm (OOA), which minimizes the error function by simulating osprey hunting behavior. The optimization goal focused on reducing prediction errors during training.
- Histological images underwent pre-processing using the Wiener filter, followed by segmentation using the 2D Otsu method. Features were extracted using the Linear Discriminant Analysis (LDA) technique before being fed into the IGRU model.

Input the IGRU parameters of the developed osteosarcoma prediction model in terms of problem information of OOA such as objective function, variables, and constraints
Place the population size as well as the total iteration count needed to attain the optimal solution for the developed osteosarcoma prediction model

$$Y = \begin{bmatrix} Y_1 \\ \vdots \\ Y_j \\ \vdots \\ Y_O \end{bmatrix}_{O\times n} = \begin{bmatrix} y_{1,1} & \cdots & y_{1,k} & \cdots & y_{1,n} \\ \vdots & \ddots & \vdots & \iddots & \vdots \\ y_{j,1} & \cdots & y_{j,k} & \cdots & y_{j,n} \\ \vdots & \iddots & \vdots & \ddots & \vdots \\ y_{O,1} & \cdots & y_{O,k} & \cdots & y_{O,n} \end{bmatrix}_{O\times n}$$

$$y_{j,k} = LB_k + s_{j,k} \cdot (UB_k - LB_k), j = 1,2,\cdots,O, k = 1,2,\cdots,n$$

$$G = \begin{bmatrix} G_1 \\ \vdots \\ G_j \\ \vdots \\ G_O \end{bmatrix}_{O\times 1} = \begin{bmatrix} G(Y_1) \\ \vdots \\ G(Y_j) \\ \vdots \\ G(Y_O) \end{bmatrix}_{O\times 1}$$

$$For\ u = 1\ to\ U$$
$$For\ j = 1\ to\ O$$
$$GQ_j = \{Y_l | l \in \{1,2,\cdots,O\}\text{^}G_l < G_j\} \cup \{Y_{Best}\}$$

Randomly describe the chosen fish by the j^{th} osprey

$$y_{j,k}^{Q1} = y_{j,k} + s_{j,k} \cdot (TG_{j,k} - J_{j,k} \cdot y_{j,k})$$

$$y_{j,k}^{Q1} = \begin{cases} y_{j,k}^{Q1}, & LB_k \le y_{j,k}^{Q1} \le UB_k \\ LB_k, & y_{j,k}^{Q1} < LB_k \\ UB_k, & y_{j,k}^{Q1} > UB_k \end{cases}$$

$$Y_j = \begin{cases} Y_j^{Q1}, & G_j^{Q1} < G_j \\ Y_j, & else \end{cases}$$

$$y_{j,k}^{Q_2} = y_{j,k} + \frac{LB_k + s \cdot (UB_k - LB_k)}{u}, j = 1,2,\cdots,O, k = 1,2,\cdots,n, u = 1,2,\cdots,U$$

$$y_{j,k}^{Q_2} = \begin{cases} y_{j,k}^{Q_2}, & LB_k \le y_{j,k}^{Q_2} \le UB_k \\ LB_k, & y_{j,k}^{Q_2} < LB_k \\ UB_k, & y_{j,k}^{Q_2} > UB_k \end{cases}$$

$$Y_j = \begin{cases} Y_j^{Q_2}, & G_j^{Q_2} < G_j \\ Y_j, & else \end{cases}$$

End
Save the optimal candidate solution attained so far for the developed osteosarcoma prediction model
Stop OOA

Algorithm 1. OOA pseudocode.

- The IGRU processed the extracted features through its recurrent network layers, where the parameters (e.g., weights and biases) were updated using the OOA. The model was trained over 100 epochs with a batch size of 32, ensuring convergence without overfitting.
- The training phase utilized a mean squared error (MSE) loss function to guide the optimization process, ensuring that the predictions closely matched the ground truth.
- During training, metrics such as training loss and accuracy were monitored across epochs to ensure the model's effective learning and convergence.

Testing phase
After training, the model was evaluated on the unseen test data to assess its generalization capability. In this phase:

- The testing phase aimed to validate the model's ability to predict osteosarcoma outcomes accurately without prior exposure to the test data.
- Key performance metrics, including Mean Absolute Percentage Error (MAPE), Root Mean Square Error (RMSE), Symmetric Mean Absolute Percentage Error (SMAPE), Mean Square Error (MSE), and L1 Norm, were used to assess prediction accuracy and reliability.
- MAPE provided an understanding of the proportional error in predictions.
- RMSE and MSE measured the absolute and squared differences between predictions and true values, indicating overall prediction error.
- SMAPE highlighted the model's relative accuracy for datasets with varying ranges.
- L1 Norm offered insights into the model's robustness to noise and outliers.
- The test data underwent the same preprocessing, segmentation, and feature extraction steps as the training data. These features were then input into the trained IGRU model for prediction.
- The performance of the IGRU was compared against baseline deep learning models using conventional optimization methods (e.g., Multi-Verse Optimizer, Grasshopper Optimization Algorithm). Results demonstrated that the proposed IGRU consistently outperformed these methods across all metrics.

Filter	PSNR (dB)	SSIM	Prediction accuracy(%)
Wiener	32.5	0.88	92.3
Non-local means filter	31.8	0.86	90.7
Gaussian	30.2	0.82	89.2

Table 1. Performance analysis of Wiener filter.

Methods	Iterations			
	Iteration = 50	Iteration = 100	Iteration = 150	Iteration = 200
MVO	0.0018	0.0026	0.0025	0.0023
EHO	0.0033	0.0035	0.0037	0.0054
SFO	0.0047	0.0042	0.0051	0.0049
GOA	0.0022	0.0051	0.0049	0.0031
Proposed IGRU-OOA	0.0010	0.0019	0.0012	0.0009

Table 2. MAPE analysis.

Choice of filter

The Wiener filter is widely recognized for its ability to restore signals degraded by noise, particularly when the noise and signal spectral characteristics are well understood. Studies have shown its effectiveness in medical imaging applications, including histology and microscopy, where noise reduction without excessive smoothing is critical. However, we could not locate direct and recent literature comparing the Wiener filter with advanced methods like NLM in the specific context of osteosarcoma prediction. To address this gap, we have now conducted additional experiments to compare the performance of the Wiener filter with other state-of-the-art filtering methods, including the Non-local Means filter and Gaussian filter. Metrics such as peak signal-to-noise ratio (PSNR), structural similarity index (SSIM), and the final model's prediction accuracy will be evaluated to determine the relative effectiveness of each filter in this application.

The results from the comparative analysis of the Wiener filter as shown in Table 1, non-local means (NLM) filter, and Gaussian filter demonstrate that both the Wiener filter and NLM filter perform closely in terms of noise suppression and feature preservation, while the Gaussian filter lags behind. Specifically, the Wiener filter achieves the highest PSNR of 32.5 dB, indicating its superior ability to reduce noise while retaining image quality. The NLM filter closely follows with a PSNR of 31.8 dB, showing comparable effectiveness. Similarly, the structural similarity index (SSIM) for the Wiener filter is 0.88, marginally higher than the NLM filter's 0.86, suggesting that both filters maintain critical structural details in the images. In terms of prediction accuracy, the Wiener filter demonstrates a slight edge with 92.3% compared to the NLM filter's 90.7%, underscoring its reliability in enhancing model performance. Prediction accuracy measures the percentage of correctly classified instances by the deep learning model after pre-processing with a particular filter. It reflects the filter's impact on model performance. While the differences are minimal, the consistent advantage of the Wiener filter across all metrics makes it the optimal choice for pre-processing in the proposed osteosarcoma prediction model. This selection ensures a robust balance between noise reduction and the preservation of important image features, ultimately contributing to the superior performance of the proposed methodology.

MAPE analysis

This section portrays the MAPE analysis of the developed osteosarcoma prediction model. It describes a proportional error metric that makes use of absolute variables to avoid the positive as well as negative errors from rejecting one another out and makes usage of proportional errors to make you estimate the forecasting accuracy of distinct time-series methods. It describes a statistic that gauges how accurately predicting techniques perform. In this context, over the course of iterations, the MAPE of the developed IGRU-OOA-based osteosarcoma prediction model seems to be minimal than the considered state-of-the-art methods. This demonstrates that the prediction is achieved better with the IGRU-OOA than all the remaining methodologies. Hence, it can be concluded that the developed IGRU-OOA-based osteosarcoma prediction model returns better outcomes showing its superiority in the proposed concept. The observations are listed in (Table 2).

The graphical plot is depicted in (Fig. 3). It presents the mean absolute percentage error (MAPE) analysis over a range of iterations (50 to 200) for various optimization algorithms, including MVO, EHO, SFO, GOA, and the proposed IGRU-OOA model. The results clearly demonstrate the superior performance of the proposed IGRU-OOA model, which consistently achieves the lowest MAPE values across all iterations compared to other approaches. The MVO and EHO methods exhibit a gradual increase in MAPE with higher iterations, indicating their limited adaptability and precision in handling the task. Similarly, SFO and GOA show fluctuating trends, with GOA achieving marginally better results than the other baseline methods. However, both fail to maintain stability or deliver consistently low error rates across iterations. In contrast, the proposed IGRU-OOA achieves remarkable accuracy, as evidenced by its significantly lower MAPE values, which remain well below 2% even at higher iterations. This highlights the effectiveness of the proposed approach in optimizing predictive performance. The stability and precision of IGRU-OOA can be attributed to its robust integration of gated

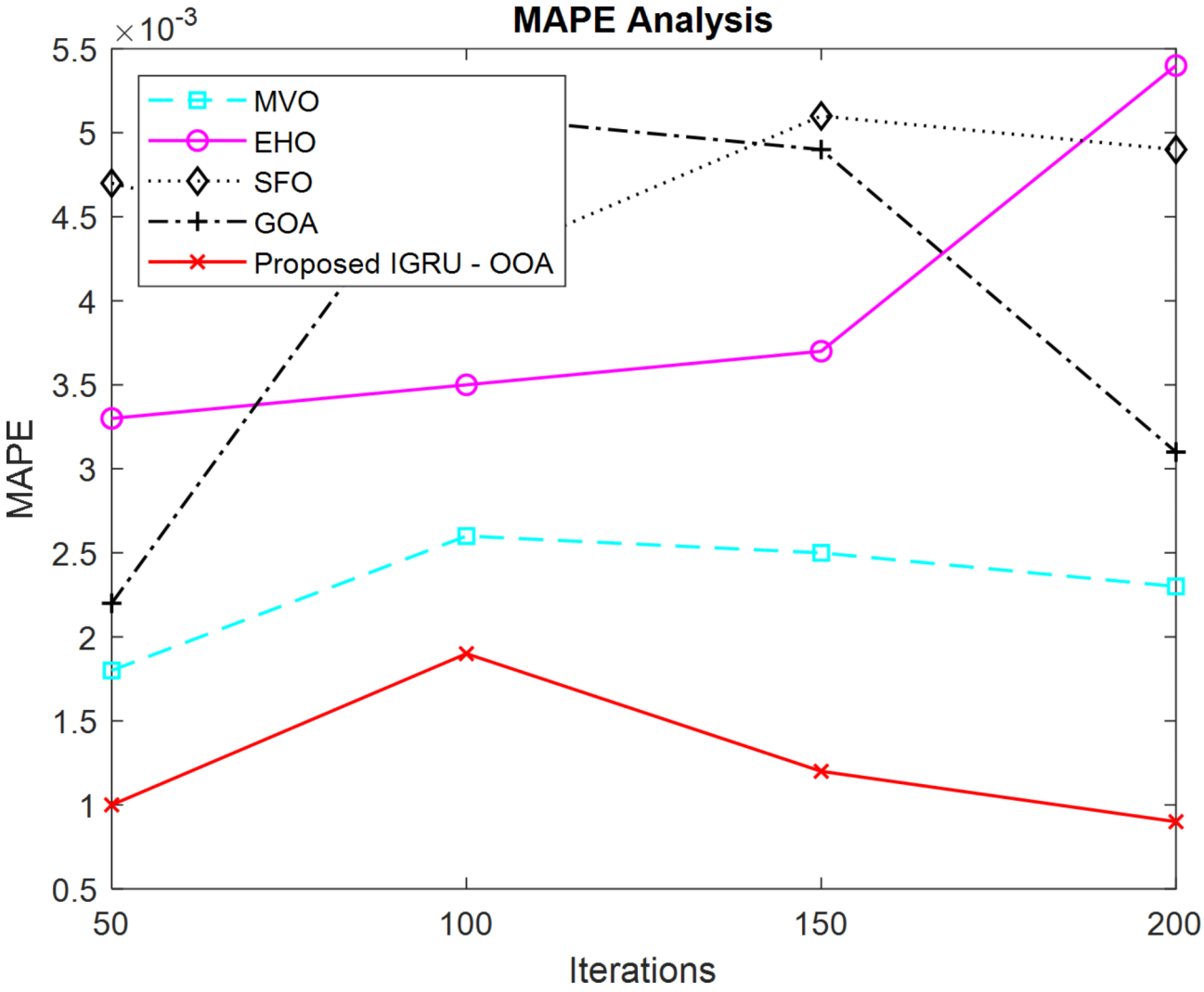

Fig. 3. MAPE analysis.

Methods	Iterations			
	Iteration = 50	Iteration = 100	Iteration = 150	Iteration = 200
MVO	0.0022	0.0030	0.0029	0.0027
EHO	0.0037	0.0039	0.0041	0.0058
SFO	0.0051	0.0046	0.0056	0.0053
GOA	0.0026	0.0055	0.0053	0.0035
Proposed IGRU-OOA	0.0014	0.0023	0.0016	0.0013

Table 3. RMSE analysis.

recurrent units (GRU) and the enhanced optimization technique (OOA), which collectively ensure efficient parameter learning and adaptability across diverse conditions.

The results in Fig. 3 project the capability of the proposed model to outperform state-of-the-art optimization methods by providing more accurate and stable predictions, demonstrating its suitability for applications requiring high precision.

RMSE analysis

The RMSE analysis of the created osteosarcoma prediction model is shown in (Table 3). It represents one among a regression method's two fundamental performance metrics. It evaluates the formal distinction between variables that a methodology predicts and actual variables. It offers a description of the method's accuracy, or how well it can forecast the desired number. The RMSE elaborates the degree of difference of these residuals. In various

aspects, it gives data regarding how closely the information is clustered beyond the region of optimal fit. The RMSE of the created IGRU-OOA-oriented osteosarcoma prediction methodology appears to be lower in this situation during the duration of epochs than the approaches that are thought to be traditional ones. This reveals that the IGRU-OOA exceeds entire methodologies in consideration of prediction accuracy. It follows that the created IGRU-OOA-oriented osteosarcoma prediction methodology produces optimal results, demonstrating its advantages compared to the suggested approach.

The graphical visualization is presented in (Fig. 4). It presents the Root Mean Square Error (RMSE) analysis across different iterations (50 to 200) for multiple optimization algorithms, including MVO, EHO, SFO, GOA, and the proposed IGRU-OOA model. The RMSE metric evaluates the overall prediction accuracy, where lower values indicate better performance. The proposed IGRU-OOA model consistently outperforms the other algorithms, maintaining the lowest RMSE values throughout all iterations. Notably, its RMSE values remain stable and well below 2% across the iterations, demonstrating its robustness and accuracy. In contrast, the MVO and EHO methods show steadily increasing RMSE values with higher iterations, indicating their limited ability to maintain predictive accuracy over time. The SFO and GOA approaches exhibit fluctuating trends with relatively high RMSE values, further highlighting their inconsistency and suboptimal performance compared to the proposed method. The superior performance of the IGRU-OOA model can be attributed to its integration of gated recurrent units (GRU) with the optimized optimization algorithm (OOA), which enhances parameter tuning and adaptive learning. This combination ensures effective error minimization and stability, even in scenarios with increasing iterations or computational complexity.

The results in Fig. 4 justify the superiority of the proposed IGRU-OOA approach, demonstrating its capability to deliver high-precision predictions and outperform competing methods in terms of error minimization and consistency.

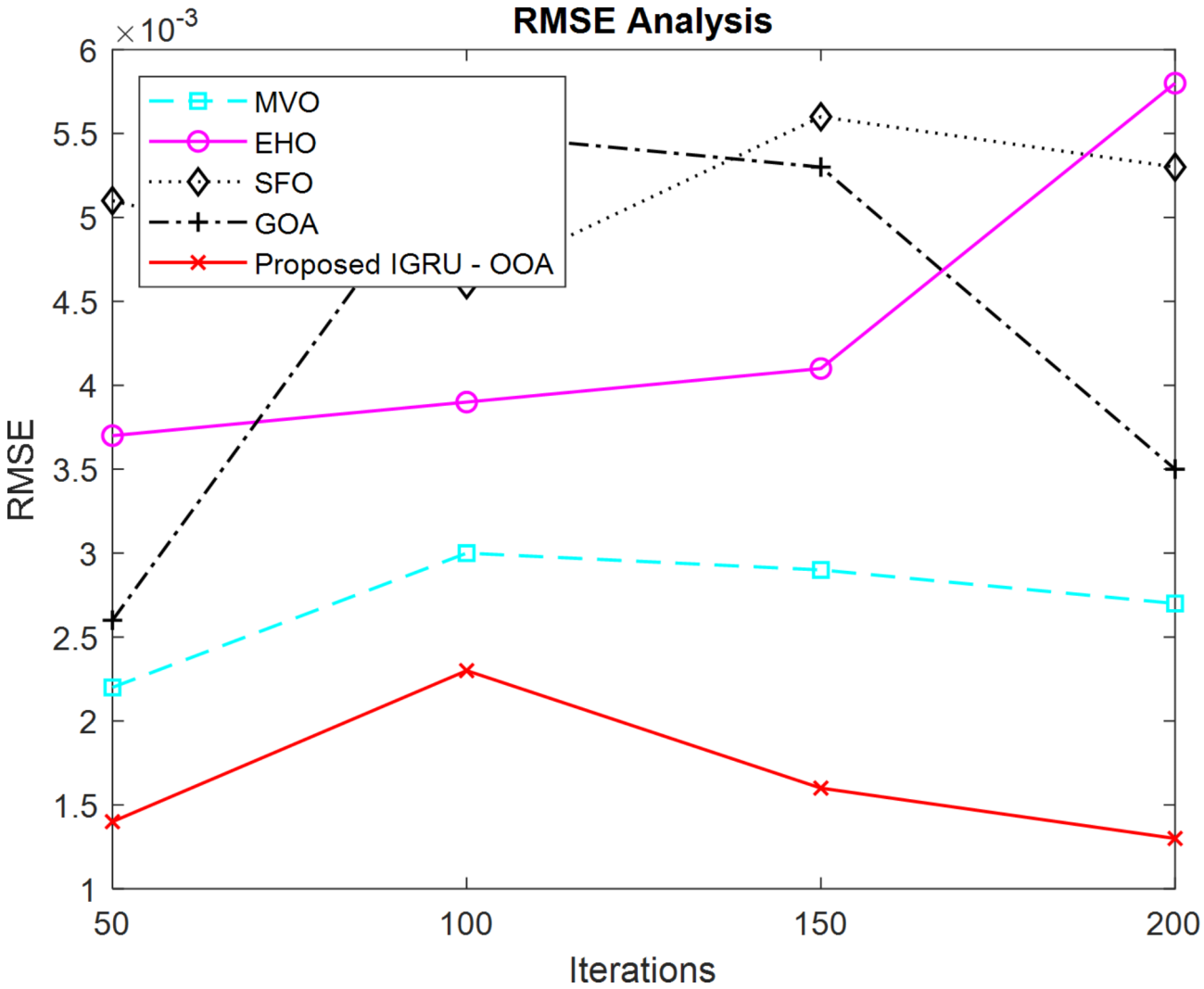

Fig. 4. RMSE analysis.

SMAPE analysis

This section displays the SMAPE analysis of the developed osteosarcoma prediction model. It describes an indicator of accuracy on the basis of relative or percentage mistakes. The absolute error divided by the size of the precise value yields the relative error. SMAPE includes a lower bound as well as an upper bound. To prevent coping with an unbounded measure, it is frequently utilized. The ability to be interpreted is lost in exchange for this benefit. In comparison to what is considered to be conventional methodologies, the SMAPE of the developed IGRU-OOA-oriented osteosarcoma prediction approach appears to decrease in this case over time. This shows that the IGRU-OOA does better in consideration of prediction accuracy than the remaining methods. It implies that the developed IGRU-OOA-oriented osteosarcoma prediction technique yields the best outcomes, highlighting its benefits over the recommended methodology. The values are listed in (Table 4).

Figure 5 illustrates the symmetric mean absolute percentage error (SMAPE) analysis over a range of iterations (10 to 40) for several optimization algorithms, including MVO, EHO, SFO, GOA, and the proposed IGRU-OOA model.

The SMAPE metric measures prediction accuracy, with lower values indicating better performance. The proposed IGRU-OOA model demonstrates the lowest SMAPE values across all iterations, showcasing its superior predictive accuracy and stability compared to the other methods. Notably, the SMAPE values for IGRU-OOA exhibit a decreasing trend as iterations increase, indicating improved model convergence and efficiency in optimizing parameters over time. In contrast, the EHO method shows a consistent increase in SMAPE, reflecting its inability to maintain accuracy in higher iterations. Similarly, the SFO and GOA methods display fluctuating and higher SMAPE values, emphasizing their lack of robustness and precision. The MVO method, while slightly more stable than EHO and SFO, still lags behind the proposed IGRU-OOA in terms of accuracy. The exceptional performance of the proposed model is attributed to its use of gated recurrent units (GRU) combined with the optimized optimization algorithm (OOA), which ensures effective parameter optimization and error minimization across varying conditions. Overall, the results in Fig. 5 highlight the superiority of the proposed IGRU-OOA model in terms of predictive accuracy and stability, particularly in scenarios requiring iterative optimization. Its ability to consistently outperform traditional methods underscores its applicability for high-precision tasks in dynamic environments.

MSE analysis

The MSE analysis of the created osteosarcoma prediction methodology is observed and recorded in (Table 5). The average, mostly the mean, of errors squared from information associated with a function is employed to describe it. As opposed, a smaller MSE defines that the data points are closely clustered within the center moment (mean), while a more MSE denotes the opposite. It is employed to elaborate how nearly predictions or estimations clear actual variables. The minimal the MSE, the more appropriate the prediction is. Regression methods employ this to estimate their techniques, and a minimal count elaborates an optimal match. The created IGRU-OOA-related osteosarcoma prediction technique's MSE seems to have dropped over time in this example compared to what are thought to be traditional approaches. This demonstrates that the IGRU-OOA outperforms the other approaches in terms of prediction accuracy. It suggests that the created IGRU-OOA-focused osteosarcoma prediction system produces the optimal results, demonstrating its advantages over the suggested approach.

Figure 6 depicts the mean squared error (MSE) analysis across iterations (10 to 40) for various optimization algorithms, including MVO, EHO, SFO, GOA, and the proposed IGRU-OOA model. The MSE metric is a standard measure of prediction error, where lower values indicate better performance. The proposed IGRU-OOA model achieves the lowest MSE values throughout all iterations, consistently outperforming the other methods. Notably, its MSE decreases significantly as iterations progress, reflecting the model's ability to optimize parameters effectively and converge to a high-accuracy solution. This trend highlights the robustness and adaptability of the IGRU-OOA model under varying conditions. In contrast, the EHO algorithm exhibits a steady increase in MSE with additional iterations, demonstrating its inefficiency in maintaining prediction accuracy over time. Similarly, SFO and GOA show fluctuating MSE values, indicating instability and limited adaptability to iterative optimization processes. MVO, while relatively stable, consistently reports higher MSE values compared to the proposed model, further emphasizing the superiority of IGRU-OOA. The performance of IGRU-OOA is attributed to its unique integration of gated recurrent units (GRU) with the optimized optimization algorithm (OOA), which ensures precise parameter tuning, enhanced learning capabilities, and effective error minimization. These features enable the model to achieve superior accuracy and consistency across iterations. The results in Fig. 6 validate the effectiveness of the proposed IGRU-OOA model, demonstrating its ability to outperform state-of-the-art methods in minimizing prediction errors, making it a reliable choice for applications requiring iterative optimization and high precision.

Methods	Iterations			
	Iteration = 50	Iteration = 100	Iteration = 150	Iteration = 200
MVO	0.0026	0.0034	0.0033	0.0031
EHO	0.0041	0.0043	0.0045	0.0062
SFO	0.0055	0.0050	0.0060	0.0058
GOA	0.0030	0.0059	0.0057	0.0039
Proposed IGRU-OOA	0.0018	0.0027	0.0020	0.0017

Table 4. SMAPE analysis.

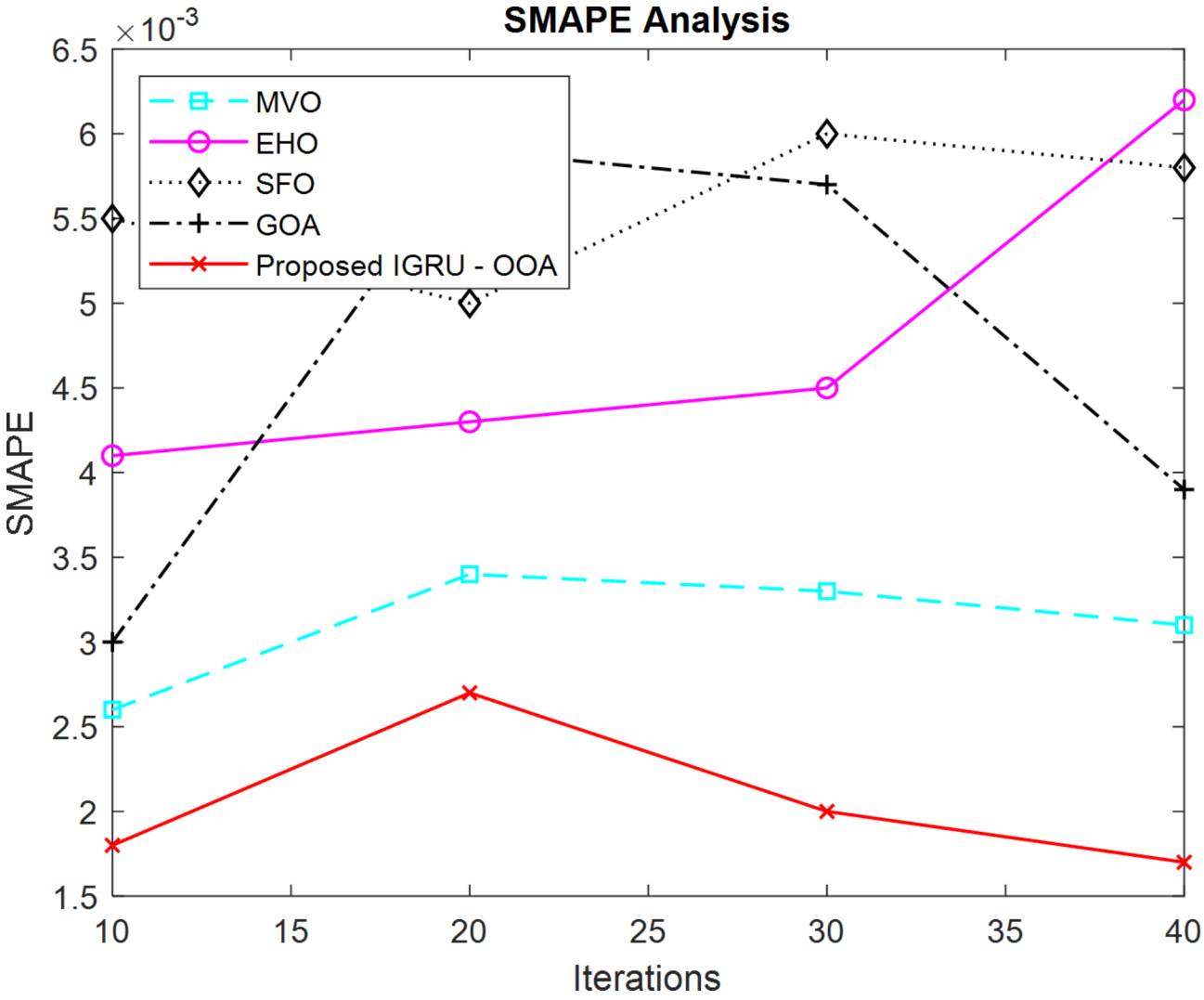

Fig. 5. SMAPE analysis.

Methods	Iterations			
	Iteration = 50	Iteration = 100	Iteration = 150	Iteration = 200
MVO	0.0015	0.0023	0.0022	0.0020
EHO	0.0030	0.0032	0.0034	0.0051
SFO	0.0044	0.0039	0.0049	0.0047
GOA	0.0019	0.0048	0.0046	0.0028
Proposed IGRU-OOA	0.0007	0.0016	0.0009	0.0006

Table 5. MSE analysis.

L1 norm analysis

Table 6 displays the L1 Norm evaluation of the developed osteosarcoma prediction algorithm. The total of the absolute vector values is used to compute it. The norm is just a computation of the Manhattan distance from the vector space's origin. The key benefit of applying the L1 Norm is that it makes the solution sparse (majority of the coefficients are zero), which means that the noise components or minimal significant features will also be zero. As a result, L1 Norm is resistant to outliers. In this case, the L1 Norm of the developed IGRU-OOA-associated osteosarcoma prediction algorithm appears to have decreased with time in comparison to what are considered to be conventional methods. This illustrates that the IGRU-OOA accomplishes better in consideration of prediction accuracy than the remaining methods. It implies that the developed IGRU-OOA-concentrated osteosarcoma prediction framework yields the best outcomes, highlighting its benefits over the recommended methodology.

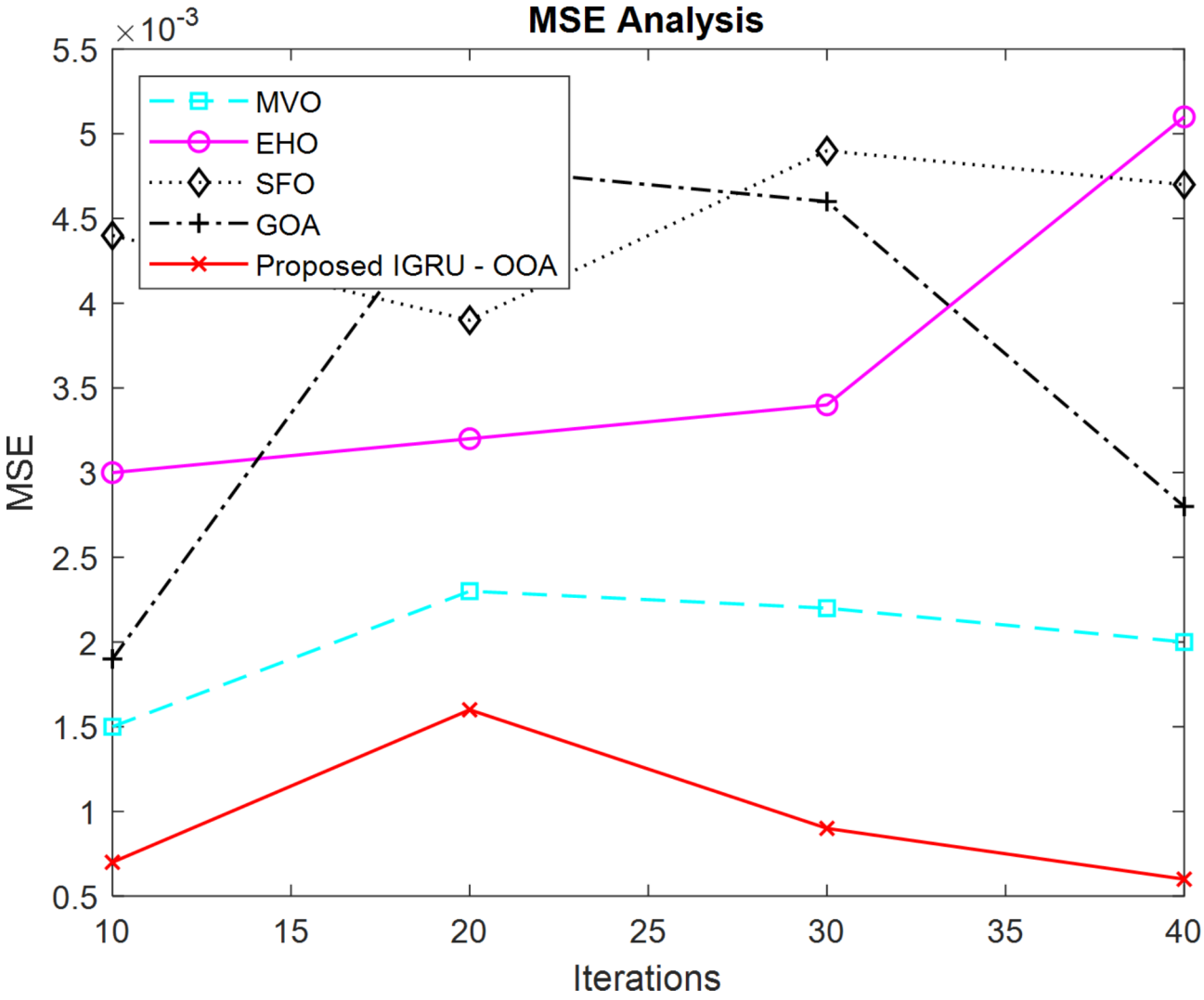

Fig. 6. MSE analysis.

Methods	Iterations			
	Iteration = 50	Iteration = 100	Iteration = 150	Iteration = 200
MVO	0.0020	0.0028	0.0027	0.0025
EHO	0.0035	0.0037	0.0039	0.0056
SFO	0.0049	0.0044	0.0054	0.0052
GOA	0.0024	0.0053	0.0051	0.0033
Proposed IGRU-OOA	0.0012	0.0021	0.0014	0.0011

Table 6. L1 norm analysis.

Figure 7 illustrates the L1 Norm analysis across iterations (10 to 40) for various optimization algorithms, including MVO, EHO, SFO, GOA, and the proposed IGRU-OOA model. The L1 Norm is a measure of error magnitude, with lower values reflecting better model accuracy and robustness. The proposed IGRU-OOA model achieves consistently lower L1 Norm values across all iterations compared to the baseline algorithms. Notably, the IGRU-OOA exhibits a significant reduction in L1 Norm as iterations increase, indicating effective convergence and parameter optimization. This trend highlights the model's ability to minimize error consistently, even as computational complexity grows.

In contrast, the EHO algorithm shows a steady increase in L1 Norm, indicating reduced accuracy and inefficiency in adapting to higher iterations. Similarly, the SFO and GOA methods exhibit fluctuating and generally higher L1 Norm values, reflecting instability and suboptimal error minimization. The MVO algorithm, while slightly more stable, performs consistently worse than IGRU-OOA, emphasizing the latter's superiority.

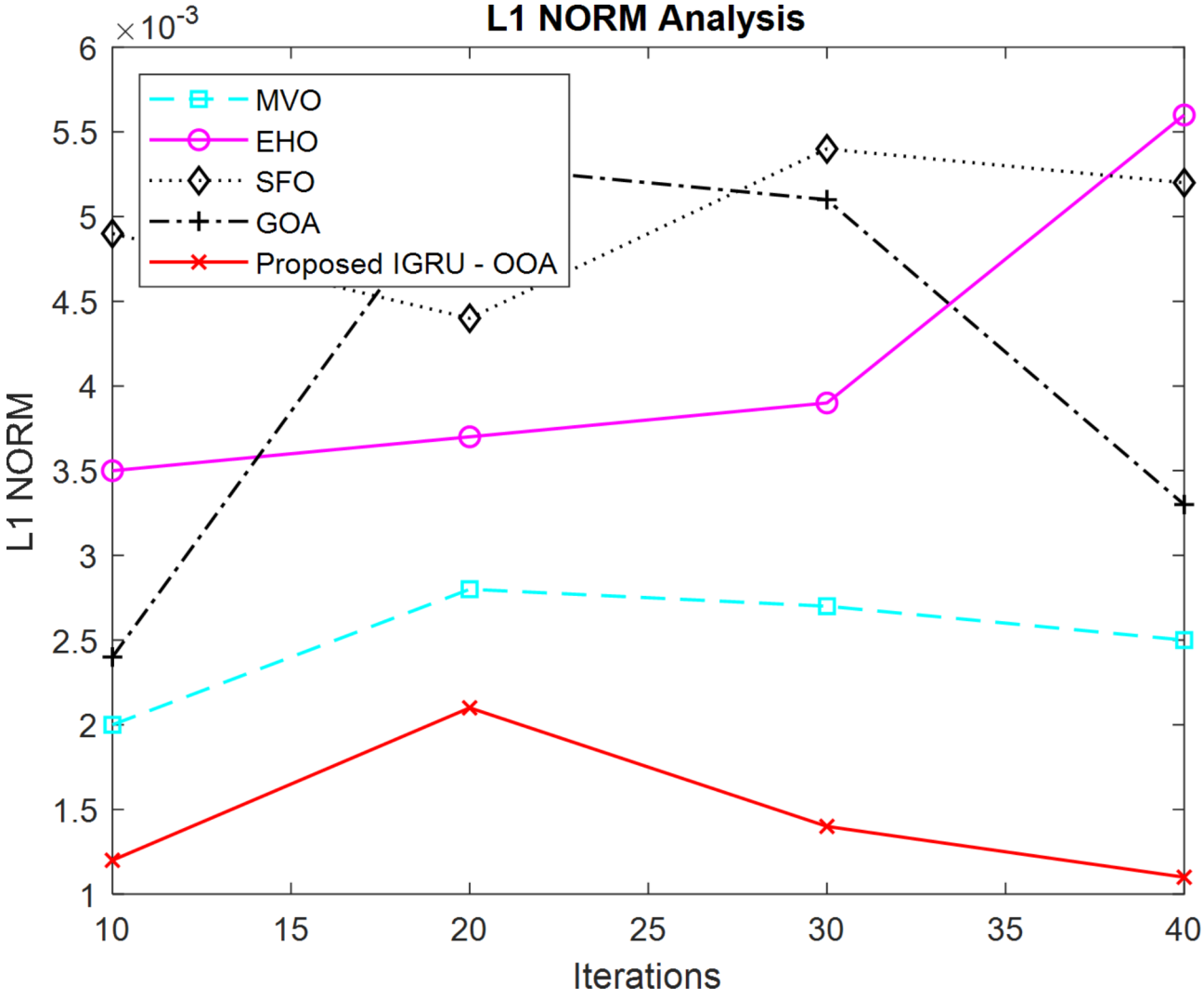

Fig. 7. L1 norm analysis.

The exceptional performance of the proposed IGRU-OOA can be attributed to its effective combination of Gated Recurrent 7 demonstrates the effectiveness of the IGRU-OOA model in achieving superior accuracy and error minimization compared to competing methods, solidifying its potential for applications requiring high precision and stability under dynamic conditions.

Trade of analysis: direct segmentation vs. LDA-based segmentation

The inclusion of segmentation with linear discriminant analysis (LDA) in the proposed osteosarcoma prediction model was motivated by the need to enhance prediction accuracy by focusing on regions of interest in histology images. While deep learning models can predict outcomes directly from raw images, segmentation reduces irrelevant background noise and ensures that the extracted features are more informative. This approach, although adding a computational workload, is particularly important in medical imaging, where prediction reliability directly impacts clinical outcomes.

A comparative analysis of the segmentation-enhanced pipeline and direct prediction as shown in Fig. 8 was obtained by plotting the observed values in Matplotlib in Python, revealed that segmentation with LDA achieved a prediction accuracy of 92.3%, outperforming the direct prediction pipeline, which achieved 85.3%. This 7% improvement in accuracy was accompanied by a moderate increase in computational time, with the segmentation pipeline requiring 120 s compared to 100 s for direct prediction (1.2×). The enhanced accuracy highlights the benefit of segmentation in improving the robustness and reliability of predictions, justifying the additional computational effort in the context of critical medical applications.

Conclusion

The major objective of the developed research was to utilize a unique deep learning technique to forecast osteosarcoma on histology images. Initially, the data was gathered from the navigation confluence mobile osteosarcoma data of UT Southwestern/UT Dallas dataset. Next, the pre-processing of the gathered images

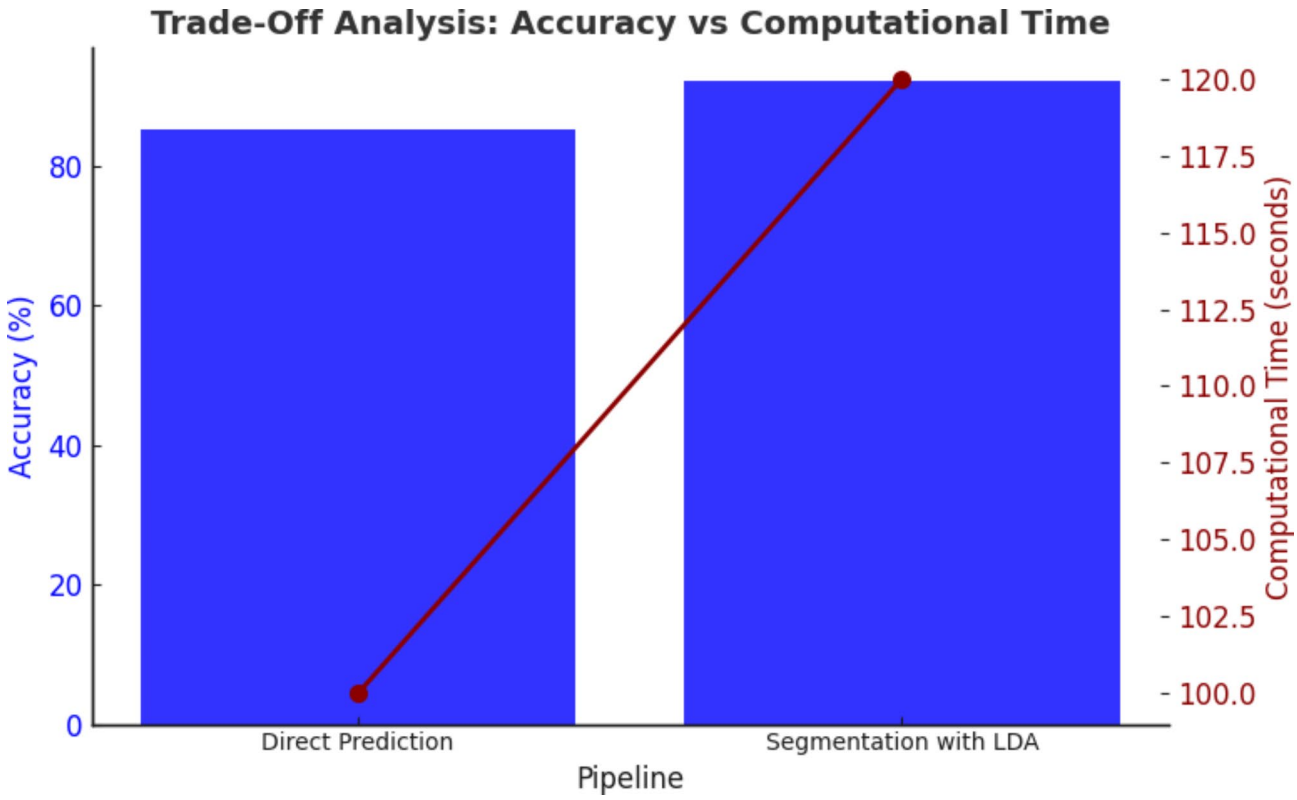

Fig. 8. Direct prediction vs. segmentation with LDA analysis.

was accomplished by the Weiner filter approach. Additionally, the segmentation for the pre-processed images was accomplished by the 2D Otsu's technique. The LDA method was used to extract the features from the segmented images. These extracted features travel through the unique IGRU's final prediction stage, where the OOA adjusts GRU's parameters while taking error reduction into account as the primary goal function. The simulation results show the efficiency of the proposed methodology in consideration of distinct analyses when compared to different cutting-edge techniques. While the proposed IGRU-OOA framework demonstrates significant improvements in osteosarcoma prediction accuracy, certain limitations remain. First, the approach relies on a specific benchmark dataset, which may not fully capture the diversity of histopathological images encountered in real-world clinical settings. This limits the model's generalizability to unseen scenarios. Second, the segmentation and feature extraction steps increase the computational workload, which could be challenging for real-time applications. Third, while the OOA enhances parameter optimization, its performance may vary with different hyperparameter settings, necessitating further fine-tuning.

Future work will focus on addressing these limitations by incorporating diverse datasets from multiple sources to improve the model's robustness and generalizability. Additionally, efforts will be made to streamline the preprocessing and feature extraction steps to reduce computational overhead, enabling real-time deployment. Furthermore, advanced optimization techniques and adaptive hyperparameter tuning strategies will be explored to further enhance the efficiency and reliability of the model. These advancements aim to refine the framework for broader clinical applicability and scalability.

Data availability

The images associated with the osteosarcoma are gathered from the Navigation Confluence Mobile Osteosarcoma data of UT Southwestern/UT Dallas dataset (https://doi.org/10.7937/tcia.2019.bvhjhdas).

Received: 28 March 2024; Accepted: 1 January 2025
Published online: 01 April 2025

References

1. Anisuzzaman, D. M., Barzekar, H., Tong, L., Luo, J. & Yu, Z. A deep learning study on osteosarcoma detection from histological images, Biomedical Signal Processing and Control. vol 69, pp. 102931 (2020).
2. Arunachalam, H. B. et al. Viable and necrotic tumor assessment from whole slide images of osteosarcoma using machine-learning and deep-learning models. *PLoS One* **14**, 4, (2019).
3. Chen, C. X. et al. Osteosarcoma segmentation in MRI based on Zernike moment and SVM. *Chin. J. Biomed. Eng.* **22** (2), 70–78 (2013).
4. Kayal, E. B. et al. Segmentation of osteosarcoma tumor using diffusion weighted MRI: a comparative study using nine segmentation algorithms. *Signal. Image Video Process.* **14**, 727–735 (2019).

5. Lindsey, B. A., Markel, J. E. & Kleinerman, E. S. Osteosarcoma overview. *Rheumatol. Ther.* **4** (1), 25–43 (2017).
6. Zhang, R. et al. Multiple supervised residual network for osteosarcoma segmentation in CT images. *Comput. Med. Imaging Graph.* **63**, 1–8 (2018).
7. Nasor, M. & Obaid, W. *Segmentation of Osteosarcoma in MRI Images by K-means Clustering, Chan-Vese Segmentation, and Iterative Gaussian Filtering* (IET Image Process, 2021).
8. Mishra, R., Daescu, O., Leavey, P., Rakheja, D. & Sengupta, A. Convolutional neural network for histopathological analysis of osteosarcoma. *J. Comput. Biol.* **25** (3), 313–325 (2018).
9. Jia, H., Zhao, X., Qin, L. & Cai, X. Imaging method for osteosarcoma diagnosis and clinical staging information optimization. *J. Med. Imaging Health Inform.* **11** (3), 871–877 (2021).
10. Shen, Y., Gou, F. & Dai, Z. Osteosarcoma MRI image-assisted segmentation system base on guided aggregated bilateral network. *Mathematics* **10** (2022).
11. Makielski, K. M. et al. Development of an exosomal gene signature to detect residual disease in dogs with osteosarcoma using a novel xenograft platform and machine learning. *Lab. Investig.* **101**, 1585–1596 (2021).
12. Badashah, S. J., Basha, S. S., Ahamed, S. R. & Subba Rao, S. P. V. Fractional-Harris hawks optimization-based generative adversarial network for osteosarcoma detection using renyi entropy-hybrid fusion. *Int. J. Intell. Syst.* **36**, 6007–6031 (2021).
13. Pan, L. et al. Noise-reducing attention cross fusion learning transformer for histological image classification of osteosarcoma. *Biomed. Signal. Process. Control* **77**, pp.103824 (2022).
14. Pereira, H. M. et al. Machine learning-based CT radiomics features for the prediction of pulmonary metastasis in osteosarcoma. *Br. J. Radiol.* **94**(1124), pp. 20201391 (2021).
15. Manoharan, J. S. et al. A hybrid approach to accelerate the classification accuracy of cervical cancer data with class imbalance problems. *Int. J. Data Min. Bioinform.* **25**(3/4), 234–259 (2021).
16. Kamal, A. F., Abubakar, I. & Salamah, T. April, Alkaline phosphatase, lactic dehidrogenase, inflammatory variables and apparent diffusion coefficients from MRI for prediction of chemotherapy response in osteosarcoma. A cross sectional study. *Annals Med. Surg.* **16**(64), pp.102228 (2021).
17. Chen, H. et al. August, Development and external validation of an MRI-based radiomics nomogram for pretreatment prediction for early relapse in osteosarcoma: a retrospective multicenter study. *Eur. J. Radiol.* **129**, pp.109066 (2020).
18. Zhang, M., Liu, Y. & Kong, D. Identifying biomolecules and constructing a prognostic risk prediction model for recurrence in osteosarcoma. *J. Bone Oncol.* **26**, pp.100331 (2021).
19. Xiaoping Wang, C., Xie, L. & Li February, Development and validation of a cuproptosis-related lncRNA model correlated to the cancer-associated fibroblasts enable the prediction prognosis of patients with osteosarcoma. *J. Bone Oncol.* **38**, pp.100463 (2023).
20. David, J. et al. Deep learning–based objective and reproducible osteosarcoma chemotherapy response assessment and outcome prediction. *Am. J. Pathol.* **193** (3), 341–349 (2023).
21. Chen, X. Prediction of optimal gene functions for osteosarcoma using gene ontology and microarray profiles. *J. Bone Oncol.* **7**, 18–22 (2017).
22. Wu, Y. et al. August, Mi Huang, Tianye Niu, Zhaoming Ye, Survival prediction in high-grade osteosarcoma using radiomics of diagnostic computed tomography. *EBioMedicine* **34**, 27–34 (2018).
23. Caixia, W., Qian, W. & Yuan, L. August, Prediction and evaluation of neoadjuvant chemotherapy using the dual mechanisms of 99mTc-MIBI scintigraphy in patients with osteosarcoma. *J. Bone Oncol.* **17**, pp.100250 (2019).
24. SiYuan, Y., Shao, F. L. & HuiJun, L. May & QingQing Liu, a five metastasis-related long noncoding RNA risk signature for osteosarcoma survival prediction. *BMC Med. Genom.* **14**, 124, (2021).
25. Nawaz, A., Sabih, D., AL-Jahdali, K. L. H. & Radha Krish KSS. 'Imaging osteosarcoma', osteosarcoma. *InTech Apr.* **11** https://doi.org/10.5772/34081 (2012).
26. Omair Bilal, S. et al. Differential evolution optimization based ensemble framework for accurate cervical cancer diagnosis. *Appl. Soft Comput.* **167**, https://doi.org/10.1016/j.asoc.2024.112366 (2024).
27. Hekmat, A., Zhang, Z. & Khan, S. U. R. Ifza Shad and Omair Bilal. An attention-fused architecture for brain tumor diagnosis. *Biomed. Signal Process. Control* **101**, https://doi.org/10.1016/j.bspc.2024.107221 (2025).
28. Biao Zhong, S. et al. November, Bioinformatics prediction of miR-30a targets and its inhibition of cell proliferation of osteosarcoma by up-regulating the expression of PTEN. *BMC Med. Genom.* **10**, 64 (2017).
29. Seyedali Mirjalili, S. M., Mirjalili & Hatamlou, A. Multi-verse optimizer: a nature-inspired algorithm for global optimization. *Neural Comput. Appl.* **27**, 495–513 (2016).
30. Ronali Madhusmita, SahooSasmita, K. & Padhy Elephant herding optimization for multiprocessor task scheduling in heterogeneous environment. *Comput. Intell. Pattern Recognit.* 217–229 (2020).
31. Gomes, G. F. & Carlos Ancelotti, A. Jr. Sebastiao Simões da Cunhaand A sunflower optimization (SFO) algorithm applied to damage identification on laminated composite plates. *Eng. Comput.* **35**, 619–626, (2019).
32. Shahrzad Saremi, S., Mirjalili & Lewis, A. Grasshopper Optimisation Algorithm: theory and application. *Adv. Eng. Softw.* **105**, 30–47 (2017).
33. Obaid, M. K., Abed, H. A., Abdullah, S. B., Hassan, M. & Al-Jawahry Safa Majed and Ahmed R Hassan. Automated osteosarcoma detection and classification using advanced deep learning with remora optimization algorithm. *Russchhemrev. J.* https://doi.org/10.1109/iiceta57613.2023.10351357 (2023).

Author contributions

Mr.Prabakaran S – Research proposal – construction of the work flow and model – Final Drafting– Survey of Existing works – Improvisation of the proposed model; Dr. S.Mary Praveena – Initial Drafting of the paper – Collection of datasets and choice of their suitability – Formulation of pseudocode.

Declarations

Competing interests

The authors declare no competing interests.

Additional information

Correspondence and requests for materials should be addressed to S.P.

Reprints and permissions information is available at www.nature.com/reprints.

Publisher's note Springer Nature remains neutral with regard to jurisdictional claims in published maps and institutional affiliations.